

## Article

# Research on the Jet Characteristics and Dephosphorization Efficiency of Converter Oxygen Lance Blowing CO<sub>2</sub>-O<sub>2</sub> Mixed Gas

Guoli Wei <sup>1,2</sup>, Changli Zhou <sup>1</sup>, Shaoyan Hu <sup>1,\*</sup> , Jun Tian <sup>1,\*</sup>, Rong Zhu <sup>3</sup>, Deyong Wang <sup>1</sup> and Qingde Zhu <sup>2</sup><sup>1</sup> School of Iron and Steel, Soochow University, Suzhou 215137, China<sup>2</sup> Hongxing Iron and Steel Co., Ltd., Jiuquan Iron and Steel Group, Jiayuguan 735100, China<sup>3</sup> School of Metallurgical and Ecological Engineering, University of Science and Technology Beijing, Beijing 100083, China

\* Correspondence: syhu616@suda.edu.cn (S.H.); jtian@suda.edu.cn (J.T.)

**Abstract:** Utilization of CO<sub>2</sub> in steelmaking process has attracted extensive attention in recent years, not only because of its social benefits, but also its better metallurgical performance. Mixing CO<sub>2</sub> with O<sub>2</sub> blown by converter oxygen lance is gradually being adopted by steelmaking plants, due to its potential of reducing consumption and improving steel quality. In the present research, effect of mixing CO<sub>2</sub> on the jet characteristics of a four-nozzle oxygen lance was studied in detail by numerical simulation, taking the combustion behavior between supersonic jets and ambient atmosphere into consideration innovatively. The simulated results showed that the combustion flame is mainly distributed in the region between multiple jets, and the high temperature flame has a noticeable influence on the low-velocity region of the jet. Due to the dilution effect of CO<sub>2</sub>, mixing CO<sub>2</sub> into the oxygen jets will reduce the maximum temperature of the flame and slow down the combustion rate. With the increase of CO<sub>2</sub> mixing ratio, the high-temperature zone of combustion flame moves away from the lance tip significantly. At the same distance from the nozzle, although mixing CO<sub>2</sub> can hardly increase the velocity magnitude of the jet, but it can achieve higher dynamic pressure, indicating stronger impacting power. Then the industrial experiment of top blowing O<sub>2</sub>-CO<sub>2</sub> was carried out in a 120-ton converter. During the blowing time of 120~300 s, the mixing ratio of CO<sub>2</sub> was 15 vol.% for better dephosphorization, and no CO<sub>2</sub> was mixed in the rest time of blowing. Due to the stronger stirring and better thermodynamics, the average [P] content in the final molten steel was decreased from 0.0155 wt.% to 0.0129 wt.%, achieving higher dephosphorization efficiency.

**Keywords:** CO<sub>2</sub> utilization; converter steelmaking; oxygen lance; jet characteristics; combustion; dephosphorization



**Citation:** Wei, G.; Zhou, C.; Hu, S.; Tian, J.; Zhu, R.; Wang, D.; Zhu, Q. Research on the Jet Characteristics and Dephosphorization Efficiency of Converter Oxygen Lance Blowing CO<sub>2</sub>-O<sub>2</sub> Mixed Gas. *Metals* **2022**, *12*, 1457. <https://doi.org/10.3390/met12091457>

Academic Editor: Hong Yong Sohn

Received: 30 July 2022

Accepted: 29 August 2022

Published: 30 August 2022

**Publisher's Note:** MDPI stays neutral with regard to jurisdictional claims in published maps and institutional affiliations.



**Copyright:** © 2022 by the authors. Licensee MDPI, Basel, Switzerland. This article is an open access article distributed under the terms and conditions of the Creative Commons Attribution (CC BY) license (<https://creativecommons.org/licenses/by/4.0/>).

## 1. Introduction

Carbon dioxide (CO<sub>2</sub>) is the by-product of economic development, population growth, urbanization, and industrialization, mainly produced by burning fossil fuels, such as coal and oil [1]. Because CO<sub>2</sub> is one of the major greenhouse gases, its rising emission has led to serious climate problems such as global warming. Under this background, reducing CO<sub>2</sub> emission and achieving CO<sub>2</sub> utilization have become a global consensus [2].

In the past decades, utilizing CO<sub>2</sub> in steelmaking process has been widely studied. It has been proved that CO<sub>2</sub> can react with the elements in molten steel, such as [C], [Fe], [Si], [Mn], and [P], etc., [3–7]. Therefore, it is possible to use CO<sub>2</sub> as an oxidant in steelmaking process. In addition, unlike the strong exothermic reactions of O<sub>2</sub> as oxidant, the reactions of CO<sub>2</sub> as oxidant are usually weak exothermic reactions or even endothermic reactions [8]. It indicates that using a mixture of CO<sub>2</sub> and O<sub>2</sub> gases as the oxidant for steelmaking is theoretically feasible, and it is helpful to control the temperature of the molten bath more effectively. Zhu et al. [9–13] carried out a lot of research on the application of CO<sub>2</sub> in steelmaking process, and proposed the CO<sub>2</sub>-O<sub>2</sub> mixed injection (COMI) process. By lab-scale

experiments, they found that blowing CO<sub>2</sub>-O<sub>2</sub> mixed gas can remove the dissolved carbon from the molten steel and achieve a smelting effect [8,9]. Industrial experiments of top blowing CO<sub>2</sub>-O<sub>2</sub> mixed gas by oxygen lance in a steelmaking converter showed that the average ratio of dust generation was reduced due to the temperature drop of hot spot zone [10–13]. Lv et al. [14,15] achieved better dephosphorization ratio in a 30-ton steelmaking converter by top blowing CO<sub>2</sub>-O<sub>2</sub> mixed gas. By the way, Zhu et al. [16] also found that blowing CO<sub>2</sub> helped to remove more nitrogen from the molten steel because of the bubble proliferation characteristic of CO<sub>2</sub>. The present research have confirmed that top blowing CO<sub>2</sub>-O<sub>2</sub> mixed gas in steelmaking converter can achieve better metallurgical performance, such as reducing raw material consumption and improving steel quality. As a result, the new technology is gradually being adopted by more and more steelmaking plants.

For the converter steelmaking process, oxygen lance is the device for top blowing O<sub>2</sub> or CO<sub>2</sub>-O<sub>2</sub> mixed gas. Generally, the converter oxygen lance contains several Laval nozzles, which are designed to transform the high-pressure gas into multiple supersonic jets [17]. The multiple supersonic jets can not only inject the gaseous oxidant into the deep molten bath for better utilization efficiency, but also stir the bath to improve the reaction kinetics [18]. Therefore, jet characteristics of the multiple supersonic jets directly affect the mixing effect, gas utilization, and dephosphorization efficiency of the converter steelmaking. In recent years, a lot of research have been carried out to reveal the influence of oxygen lance structure on jet characteristics, such as nozzle design parameters, nozzle geometry, and nozzle location [19–22]. Nonomura et al. [23,24] found that unreasonable nozzle design parameters would cause the jet in a state of over-expansion or under-expansion at the nozzle exit, leading to the generation of shock wave and additional energy loss. Li et al. [25] studied the effects of nozzle inclination angles and nozzle numbers on jet coalescence phenomenon by numerical simulation method. In addition to the oxygen lance structure, environmental factors also have a significant influence on the jet characteristics. Based on the validated numerical simulation results of a single-nozzle jet, Alam et al. [26] found that the potential core length of the supersonic jet is 2.5 times longer at 1800 K than that at room temperature. Hu et al. [27,28] studied the influence of ambient temperature on the multiple-nozzle jets, and found that not only the jets attenuation was restrained, but also the coalescence between multiple jets was suppressed in high temperature environment. Numerical simulation on the multiple jets-molten steel bath interaction inside a 110-ton converter showed that the penetration depth of the multiple jets increased from 0.11035 m to 0.14807 m when the ambient temperature was raised from 300 K to 1723 K. Besides the influence of ambient temperature, Sumi et al. [29,30] reported that the velocity attenuation of a single-nozzle jet was restrained and the potential core length of the supersonic jet was also extended under reduced pressure.

In fact, the multiple supersonic jets generated by converter oxygen lance flow in the converter furnace, which is a high temperature, high carbon monoxide (CO) concentration environment [31]. Although the influence of temperature on jet characteristics has been clarified, but previous research ignores the existence of CO and the possible combustion reaction between environmental CO and top blown O<sub>2</sub>. By the way, mixing CO<sub>2</sub> into top blowing O<sub>2</sub> will inevitably affect the combustion behavior and flow behavior of the jets.

In this research, a three-dimensional numerical model was established based on the real four-nozzle oxygen lance used in a 120-ton converter, and the gas phase combustion mechanism was introduced into the mathematical models innovatively. The features of combustion field and the jet characteristics before and after ignition were studied first. Then the effects of CO<sub>2</sub>-O<sub>2</sub> mixing ratio on jets combustion and jets flow were analyzed in detail. Finally, industrial experiment of top blowing CO<sub>2</sub>-O<sub>2</sub> mixed gas was carried out in the 120-ton converter, dephosphorization rate was discussed.

## 2. Numerical Simulation

### 2.1. Geometric Model and Grid Partition

Geometric model of a commercial four-nozzle oxygen lance was established to study the jet characteristics. Figure 1a shows the design drawing of the four-nozzle oxygen lance, containing the detailed structure and dimensional parameters, and Figure 1b shows the actual picture of the lance installed in the steelmaking plant. In order to get more accurate simulation results, a highly simulated three-dimensional geometric model of the oxygen lance was established. Considering the symmetrical structure of the four-nozzle lance, only one quarter of the total domain was built and simulated, as shown in Figure 2, which helped to refine the computational domain grid and save the computing time. By setting the side walls of the computational domain as symmetry, the virtual complete oxygen lance can be obtained by mirroring in the CFD software. In previous research on the free jets of multi-nozzle oxygen lance, the simplified approach has been widely used. Recently, Zhao et al. [32] carried out both jet measurement experiments and numerical simulations to study the behaviors of supersonic oxygen multi-jets with various preheating temperatures, and validated the accuracy of the simplified approach by comparing the simulated results and the experimental results.

In order to show the structure of the geometric model more intuitively, both the actual built 1/4 model and the symmetrically displayed 1/2 model are shown in Figure 2. Apart from the water-cooling channel used for cooling the lance, which has little effect on the jet characteristics, other configuration and size are all consistent with the actual lance.

Computational domain includes the four-nozzle oxygen lance and the jet flow zone. The jet flow zone is a 1/4 cylinder with a height of 3000 mm and a radius of 1500 mm. Structured non-uniform grid system was used to mesh the whole computational domain. Mesh refinement was well performed to capture the sharp oscillation of the jet flow and combustion flame near the nozzle exit. A mesh configuration with 756,274 cells was adopted in this simulation, detailed grid arrangement of which is shown in Figure 3. The total number of cells is sufficient to get clear flow field and combustion field.

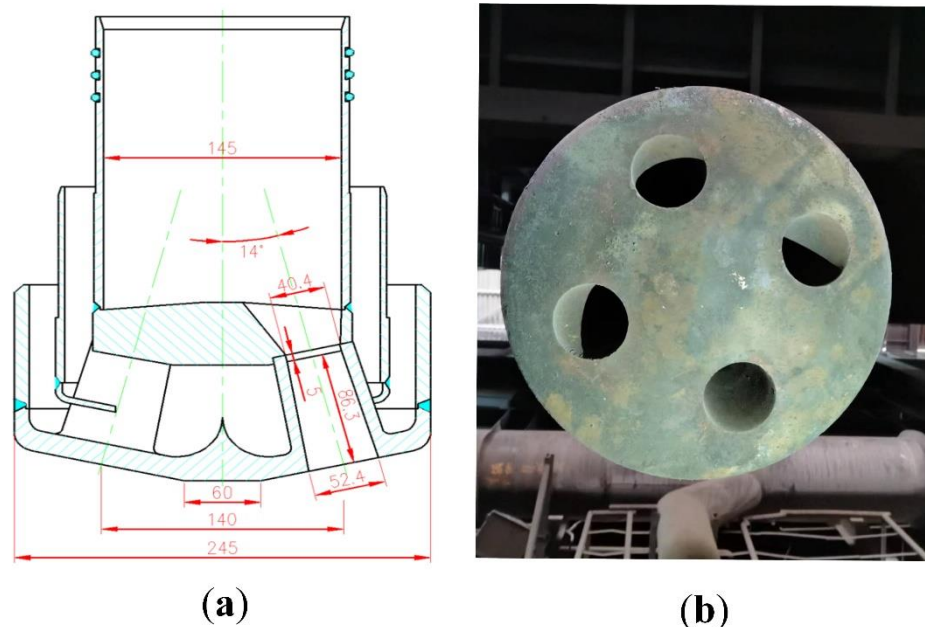


**Figure 1.** Prototype of the four-nozzle oxygen lance: (a) design drawing of the lance (unit: mm); (b) actual picture of the lance.

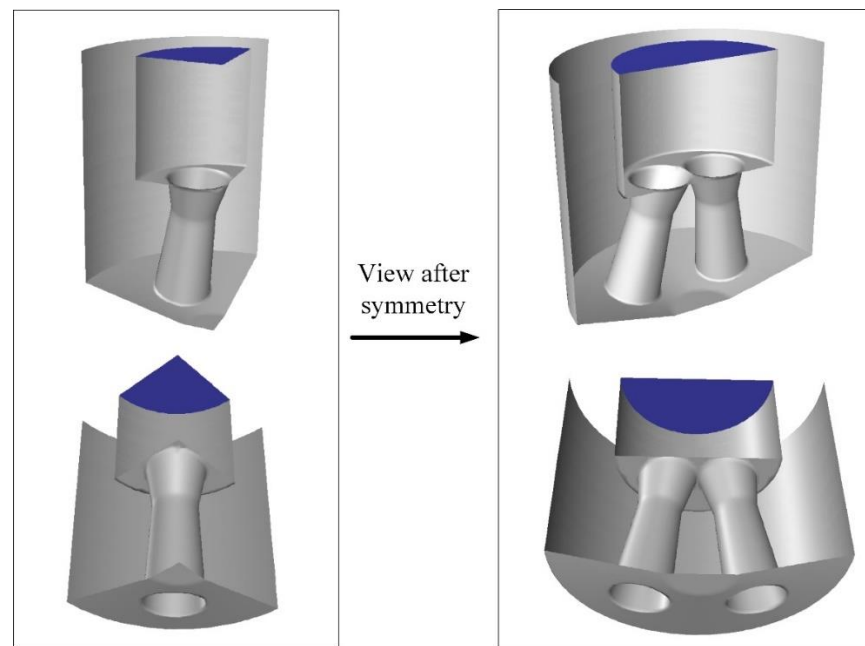


**Figure 2.** Geometric model of the oxygen lance established in present research.

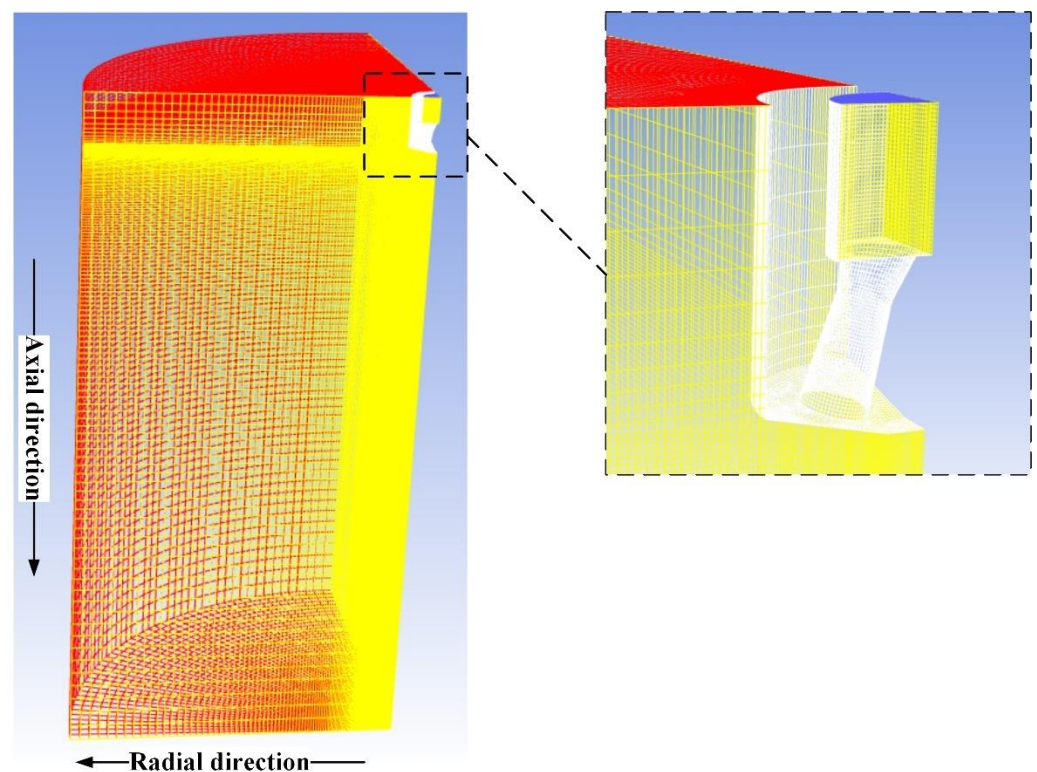


**Figure 3.** Detailed grid arrangement of the whole computational domain.

## 2.2. Simulation Schemes and Calculation Procedure

Because  $\text{CO}_2\text{-O}_2$  mixing ratio was the main research variable of this paper, four groups of simulation schemes were designed. Total volume flow rate of the  $\text{CO}_2\text{-O}_2$  mixed gas into oxygen lance was kept constant at  $24,000 \text{ Nm}^3 \cdot \text{h}^{-1}$ , volume fractions of  $\text{CO}_2$  were designed to be 0, 5 vol.%, 10 vol.%, and 15 vol.%, respectively. In order to simulate the atmosphere inside converter furnace, ambient environment of the multiple jets was assumed to be filled with high-temperature CO gas. Specific simulation schemes are shown in Table 1. In view

of the influence of high pressure, high temperature and other factors on the thermophysical properties of gas phase, all the gas species used in the simulation were treated as ideal gas.

**Table 1.** Detailed parameters of the numerical simulation schemes.

No.	Total Flow Rate of the CO <sub>2</sub> -O <sub>2</sub> Mixed Gas	Mixing Ratio of CO <sub>2</sub>	Setting Flow Rate of CO <sub>2</sub>	Setting Flow Rate of O <sub>2</sub>
1	24,000 Nm <sup>3</sup> ·h <sup>-1</sup>	0	0	24,000 Nm <sup>3</sup> ·h <sup>-1</sup>
2	24,000 Nm <sup>3</sup> ·h <sup>-1</sup>	5 vol.%	1200 Nm <sup>3</sup> ·h <sup>-1</sup>	22,800 Nm <sup>3</sup> ·h <sup>-1</sup>
3	24,000 Nm <sup>3</sup> ·h <sup>-1</sup>	10 vol.%	2400 Nm <sup>3</sup> ·h <sup>-1</sup>	21,600 Nm <sup>3</sup> ·h <sup>-1</sup>
4	24,000 Nm <sup>3</sup> ·h <sup>-1</sup>	15 vol.%	3600 Nm <sup>3</sup> ·h <sup>-1</sup>	20,400 Nm <sup>3</sup> ·h <sup>-1</sup>

To reveal the features of combustion field and its influence on jet characteristics, the scheme of blowing pure O<sub>2</sub> was selected for comparative analysis. First, this scheme was calculated without activating combustion model. In this situation, although O<sub>2</sub> and CO coexist in the computational domain, there is no combustion reaction between them. Then the combustion model was activated to get the simulation results with combustion. It should be emphasized that the only difference between the above two cases is whether to activate the combustion model, and all other conditions remain the same. Except for the scheme of blowing pure O<sub>2</sub>, all other schemes of blowing CO<sub>2</sub>-O<sub>2</sub> mixed gas were only calculated with activating combustion model.

In this research, boundary conditions of the computational domain borders were set to agree with the actual situation. The boundary type of “mass flow inlet” was applied to the gas entrance of oxygen lance. Setting values of the gas flow rate and gas composition were determined according to the simulation schemes. The boundary type of “no-slip wall” was applied to all the walls of oxygen lance, wall temperature of which were set to 300 K constantly due to the water cooling. Because this research was to study the free jet, the boundary type of “pressure outlet” was applied to all other borders. Pressure of the backflow was set to 101,325 Pa, temperature of the backflow was set to 1873 K, and species of the backflow was set to carbon monoxide.

### 2.3. Governing Equations and Turbulence Model

In the present research, the following governing equations were adopted.

Continuity equation:

$$\frac{\partial \rho}{\partial t} + \nabla \cdot (\rho U) = 0 \quad (1)$$

Momentum conservation equation:

$$\frac{\partial}{\partial t} \rho U + \nabla \cdot (\rho U \times U) - \nabla \cdot (\mu_{eff} \nabla U) = -\nabla P + \nabla [\mu_{eff} (\nabla U)] + B \quad (2)$$

Energy equation

$$\frac{\partial}{\partial t} \rho H + \nabla \cdot \rho U H - \nabla \cdot \lambda \nabla T = \frac{\partial P}{\partial t} \quad (3)$$

State equation of ideal gas:

$$P = \rho RT \quad (4)$$

In Equations (1)–(4),  $\rho$  is the average density of the fluid, kg·m<sup>-3</sup>;  $t$  is the time, s;  $U$  is the instantaneous velocity of fluid, m·s<sup>-1</sup>;  $P$  is the static pressure, Pa;  $\mu_{eff}$  is the effective viscosity, Pa·s;  $B$  is the body force, N;  $H$  is the total enthalpy, J·mol<sup>-1</sup>;  $\lambda$  is the thermal conductivity, W·m<sup>-1</sup>·K<sup>-1</sup>;  $T$  is the temperature, K; and  $R$  is the gas constant, J·kg<sup>-1</sup>·K<sup>-1</sup>.

A modified  $k$ - $\varepsilon$  model [33] with a standard wall function was used to model the turbulent flows, which is a semi-empirical model based on model transport equations for the turbulence kinetic energy ( $k$ ) and its dissipation rate ( $\varepsilon$ ).

$$\frac{\partial(\rho k)}{\partial t} + \frac{\partial(\rho k u_i)}{\partial x_i} = \frac{\partial}{\partial x_j} \left[ \left( \mu + \frac{\mu_t}{\sigma_k} \right) \frac{\partial k}{\partial x_j} \right] + G_k + G_b - \rho \varepsilon - Y_M + S_k \quad (5)$$

$$\frac{\partial(\rho \varepsilon)}{\partial t} + \frac{\partial(\rho \varepsilon u_i)}{\partial x_i} = \frac{\partial}{\partial x_j} \left[ \left( \mu + \frac{\mu_t}{\sigma_\varepsilon} \right) \frac{\partial \varepsilon}{\partial x_j} \right] + C_{1\varepsilon} \frac{\varepsilon}{k} (G_k + C_{3\varepsilon} G_b) + C_{2\varepsilon} \rho \frac{\varepsilon^2}{k} + S_\varepsilon \quad (6)$$

where  $u_i$  is the flow velocity of fluid in the direction  $i$ ,  $\text{m}\cdot\text{s}^{-1}$ ;  $x_i$  and  $x_j$  are the Cartesian coordinates in the  $i$  and  $j$  directions, respectively;  $\mu_t$  is the turbulent viscosity coefficient;  $\mu$  is the turbulent dynamic viscosity,  $\text{Pa}\cdot\text{s}$ ;  $G_k$  is the generation of turbulence kinetic energy owing to the mean velocity gradients,  $\text{J}$ ;  $G_b$  is the generation of turbulence kinetic energy caused by buoyancy,  $\text{J}$ ;  $Y_M$  is the contribution of the fluctuating dilatation in compressible turbulence to the overall dissipation rate;  $C_{1\varepsilon}$ ,  $C_{2\varepsilon}$ ,  $C_{3\varepsilon}$ , and  $C_\mu$  are constants;  $\sigma_k$  and  $\sigma_\varepsilon$  are the turbulent Prandtl numbers for  $k$  and  $\varepsilon$ , respectively; and  $S_k$  and  $S_\varepsilon$  are user-defined source terms. The model constants  $C_{1\varepsilon}$ ,  $C_{2\varepsilon}$ ,  $C_{3\varepsilon}$ ,  $C_\mu$ ,  $\sigma_k$  and  $\sigma_\varepsilon$  are usually given as follows:  $C_{1\varepsilon} = 1.44$ ,  $C_{2\varepsilon} = 1.92$ ,  $C_\mu = 0.09$ ,  $\sigma_k = 1.0$  and  $\sigma_\varepsilon = 1.3$ . The turbulent viscosity coefficient  $\mu_t$  can be computed as:

$$\mu_t = \rho C_\mu \frac{\varepsilon^2}{k} \quad (7)$$

#### 2.4. Combustion Model and Radiation Model

Generally, there are two typical approaches to model the gas phase combustion: the Eddy Dissipation Concept (EDC) model and Eddy Dissipation/Finite Rate (ED/FR) model. The EDC model takes the chemical representation and turbulence-chemistry interaction into consideration, and assumes that reactions occur in small structure, at the so-called fine scales. Combustion at the fine scales is assumed to occur as a constant pressure reactor. The evolution of species concentration is computed by integrating the chemistry within those fine scales [34]. Plenty of research [34–41] have proved that the EDC model can provide more accurate simulation results. Therefore, the EDC model with an overall and detailed chemical kinetic mechanism (DRM-19) was applied to study the combustion behavior of supersonic jet and ambient environment. The reaction mechanism consists of 21 species and 84 elementary reactions.

In the EDC model, species conservation equation for chemical species are as follows:

$$\frac{\partial}{\partial t} (\rho Y_i) + \nabla \cdot (\rho \vec{v} Y_i) = -\nabla \cdot \vec{J}_i + R_i \quad (8)$$

where  $Y_i$  is the local mass fraction of each species ( $i$ );  $\vec{v}$  is the velocity vector;  $\vec{J}_i$  is the diffusion flux of species; and  $R_i$  is the net rate of production of species by the chemical reaction. The length fraction of the fine scale ( $\xi$ ) and residence chemical time scale ( $\tau$ ) of the fluid in the fine structures are expressed by:

$$\xi = C_\xi \left( \frac{v \varepsilon}{k^2} \right)^{\frac{1}{2}}, \tau = C_\tau \left( \frac{v}{\varepsilon} \right)^{\frac{1}{2}} \quad (9)$$

where  $C_\xi$  and  $C_\tau$  are time scale constants equal to 2.138 and 0.408, respectively. The chemistry source term ( $R_i$ ) for each species is computed as:

$$R_i = \frac{\rho \xi^2}{\tau (1 - \xi^3)} (Y_i^* - Y_i) \quad (10)$$

where  $Y_i^*$  is the fine scale species mass fraction after reacting over the time ( $\tau$ ). The evolution of  $Y_i^*$  depends also on the chemical kinetic mechanism.

According to the research of Christo et al. [39–41], there is a marginal difference between the results calculated with and without considering the influence of radiation, especially in high-temperature environment. In order to obtain more accurate combustion field, the discrete ordinate (DO) radiation model with the weight sum of the gray gas model (WSGGM) [41] was applied.

### 2.5. Model Validation

Numerical simulation is a common method to study the supersonic oxygen jet, including the single-nozzle jet applied to electric arc furnace steelmaking and the multi-nozzle jets applied to converter steelmaking. Lots of studies [18–22,24–30] have validated the turbulence flow model used in present research, by comparing the simulated results and experimental results. In addition, plenty of research [34–41] have proved that EDC model coupled with detailed chemical mechanism can provide accurate simulation results of combustion. For instance, Li et al. [35–37] carried out a lot of simulation works and experiments on gas fuel combustion in recent years, whose results verified the model well. Hu et al. [34] used the model to study the combustion behavior and jet characteristics of single-nozzle coherent jet, which was also well validated by a jet measurement experiment.

## 3. Results of the Numerical Simulation

### 3.1. Features of Combustion Field and Its Influence on Jet Characteristics

#### 3.1.1. Features of Combustion Field

As mentioned above, in order to reveal the features of combustion field, the scheme of blowing pure O<sub>2</sub> was selected for comparative analysis. Figure 4 shows the temperature field distributions in the longitudinal section of the computational domain, in which Figure 4a shows the temperature field distribution before activating the combustion model, and Figure 4b shows the temperature field distribution after activating the combustion model. As shown in Figure 4, the temperature field changes significantly after activating the combustion model. Before activating the combustion model, maximum temperature of the whole computational domain is 1873 K, which is just the environmental temperature set by the research. After activating the combustion model, combustion reaction between the supersonic oxygen jet and the ambient environment occurs, forming the combustion flame, whose maximum temperature reaches 3150 K.

To analyze the combustion field more comprehensively, temperature field distributions in a series of cross sections are shown in Figure 5. The distances between the cross sections and the oxygen lance tip are 1000 mm, 1500 mm, 2000 mm, and 2500 mm. As can be seen from Figures 4 and 5, center of supersonic jet is the position with the lowest temperature, whether the combustion model is activated or not. With the increase of axial distance, temperature of the jet center increases gradually, but still the lowest temperature position remains in the same horizontal plane. More importantly, under the condition of activating combustion model, the combustion flame is mainly distributed in the area between multiple jets, that is, the area around the centerline of oxygen lance. Inner side of the jet starts to burn within a short distance from the lance tip, while the outer side of the jet starts to burn at a long distance, more than 2000 mm. This indicates that inner side of the supersonic jet is easier to be ignited than the outer side for the multi-nozzle oxygen lance.

In order to quantitatively describe the flame feature, temperature variations on the centerline of oxygen lance are plotted in Figure 6. For the case without combustion, temperature on the centerline decreases slowly with the increase of axial distance, mainly because the low-temperature jet gradually converges toward the centerline. For the case with combustion, temperature on the centerline first rises rapidly and then tends to be stable, mainly because the gas phase is ignited instantly.

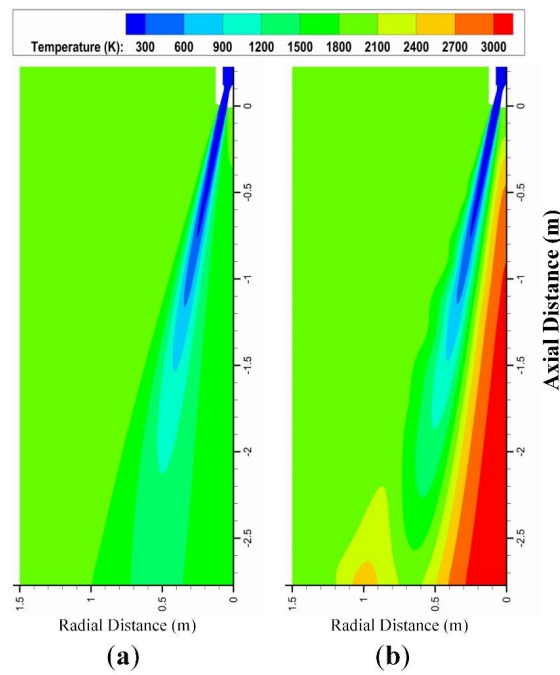


**Figure 4.** Temperature field distributions in the longitudinal section of the computational domain: (a) before activating the combustion model; (b) after activating the combustion model.

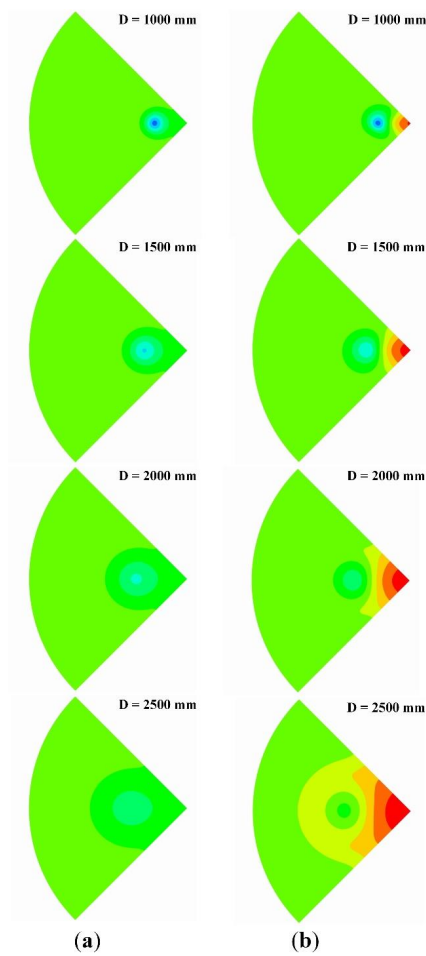


**Figure 5.** Temperature field distributions in the cross sections: (a) before activating the combustion model; (b) after activating the combustion model.

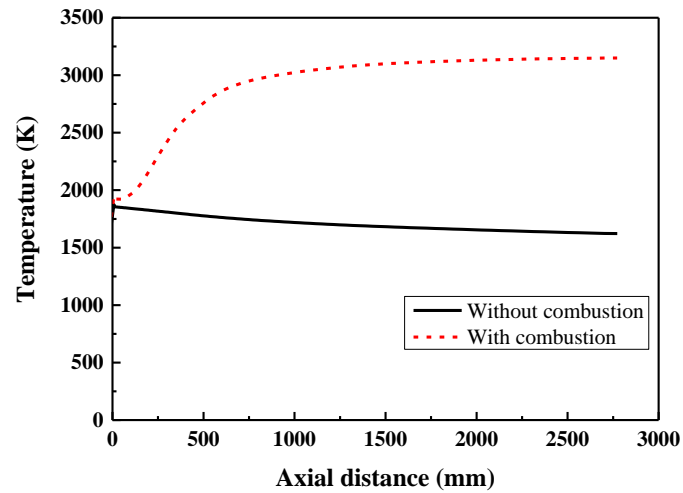


**Figure 6.** Temperature variations on the centerline of oxygen lance.

### 3.1.2. Influence of Combustion on Jet Characteristics

The change of temperature field will inevitably affect the flow of multiple supersonic jets. Velocity field distributions in the longitudinal section of computational domain is presented in Figure 7. First, whether the combustion model is activated or not, the calculated maximum velocity magnitudes in the computational domain are both  $513 \text{ m}\cdot\text{s}^{-1}$ . It is mainly because that the maximum velocity of jet appears at the nozzle exit of oxygen lance, while the combustion occurs at a distance from lance tip. Therefore, even if the combustion occurs, it can hardly affect the maximum velocity of the jet. Actually, not only the maximum velocity, but also its influence on the high-velocity region of the jet is small. For instance, as shown in Figure 7, about the region with velocity larger than  $350 \text{ m}\cdot\text{s}^{-1}$ , both the length and diameter of the jet change little after activating the combustion model. As a contrast, the influence of combustion on low-velocity region of the jet is more obvious, such as the region with velocity larger than  $200 \text{ m}\cdot\text{s}^{-1}$ .

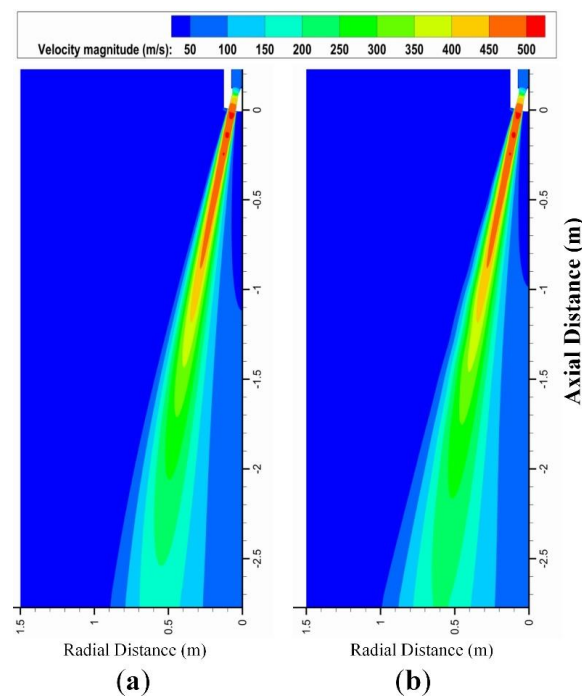


**Figure 7.** Velocity field distributions in the longitudinal section of the computational domain: (a) before activating the combustion model; (b) after activating the combustion model.

In order to quantitatively clarify the above phenomenon and law, velocity distributions on the radial directions 1500 mm and 2500 mm away from the lance tip are plotted in Figure 8. It can be seen from Figure 8a, on the radial direction 1500 mm away from the lance tip, both the velocity of jet center and the diameter of jet increase only a little after activating the combustion model. However, on the radial direction 2500 mm away from the lance tip, velocity of jet center and diameter of jet increases obviously. The velocity of jet center increases from  $204 \text{ m}\cdot\text{s}^{-1}$  to  $222 \text{ m}\cdot\text{s}^{-1}$ .

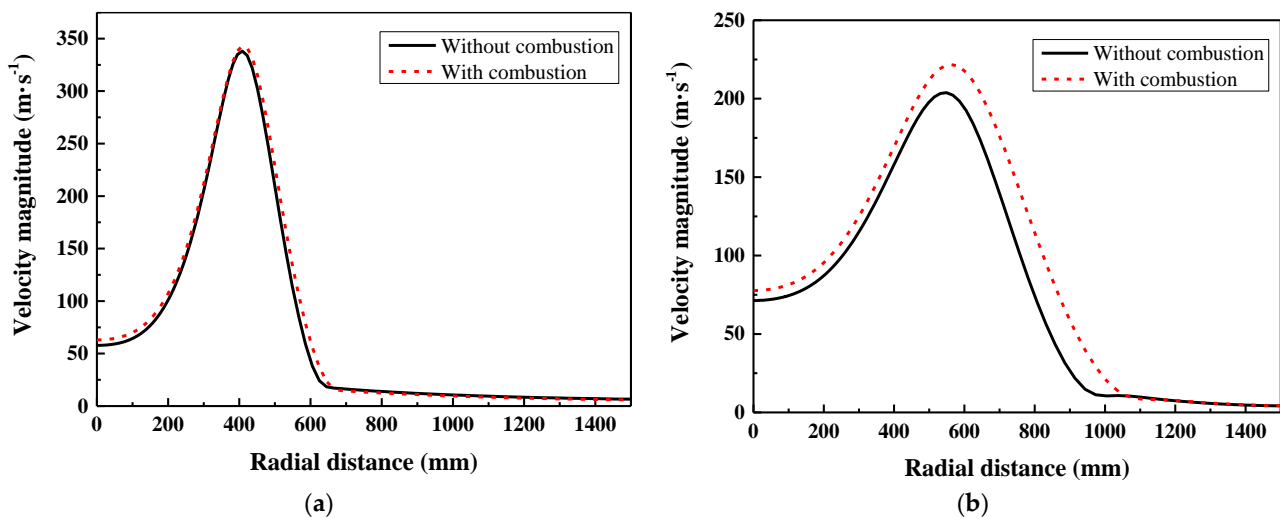


**Figure 8.** Velocity distributions on the radial directions: (a) 1500 mm away from the lance tip; (b) 2500 mm away from the lance tip.

Combined with the analysis of combustion temperature field shown in Figures 4 and 6, the reason for the above phenomenon is thought to be that the temperature in the area between multiple jets gets higher gradually with the increase of axial distance from lance tip. When the axial distance from lance tip is short, the gas phase has not been ignited or not fully burned, and the interaction time between jet and combustion flame is very short, leading to the minor influence on the high-velocity region of the jet. With the increase of axial distance from lance tip, the flame temperature increases, the jet velocity decreases, the interaction between jet and combustion flame gets more sufficient. On the one hand, according to the ideal gas state equation, the high-temperature flame causes the density of ambient environment to decrease, which helps to reduce the momentum loss of jet entrainment. On the other hand, the high-temperature flame has a heating effect on the jet, and the jet expands when heated, which also slows down the velocity attenuation. Therefore, as the axial distance from the lance tip increases, the influence of combustion on jet velocity field becomes more and more significant, meanwhile higher velocity of jet center can be obtained.

### 3.2. Effects of $\text{CO}_2\text{-O}_2$ Mixing Ratio on Jet Characteristics

The above analysis confirms that the combustion reaction between the supersonic jet and the ambient environment has a noticeable influence on the jet characteristics, which cannot be ignored. In this section, the effects of  $\text{CO}_2\text{-O}_2$  mixing ratio on jet characteristics will be discussed. It should be noted that all the cases were calculated under the condition of activating the combustion model.

#### 3.2.1. Combustion Field Analysis

Figure 9 shows the temperature field distributions in the longitudinal section of the cases with different  $\text{CO}_2\text{-O}_2$  mixing ratio. It can be found that the basic features of the combustion field are consistent with the law summarized above, combustion flame is mainly distributed in the area between multiple jets. However, the mixing ratio of  $\text{CO}_2\text{-O}_2$

has an obvious effect on the temperature field, especially on the area of high temperature zone. As the CO<sub>2</sub> mixing ratio increases, the high temperature zone gradually moves away from the lance tip, although the ignition position has not changed much. The increase of distance between lance tip and high temperature zone is beneficial to reduce the heat flux intensity of lance tip and prolong the service life of oxygen lance.

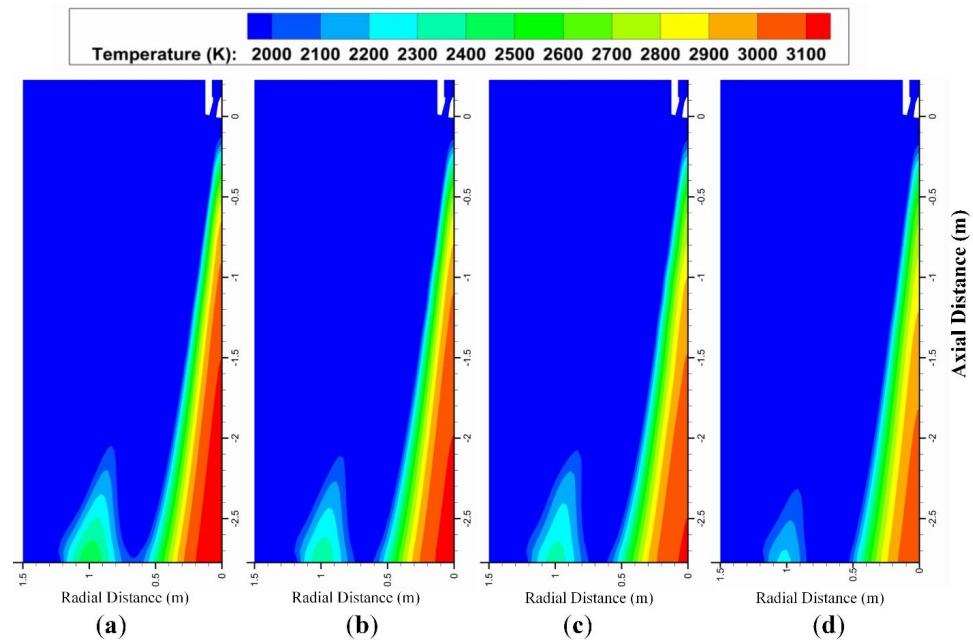


**Figure 9.** Temperature field distributions of the cases with different CO<sub>2</sub>-O<sub>2</sub> mixing ratio: (a) No CO<sub>2</sub> mixed; (b) 5 vol.% CO<sub>2</sub> mixed; (c) 10 vol.% CO<sub>2</sub> mixed; (d) 15 vol.% CO<sub>2</sub> mixed.

Temperature variations on the centerline of oxygen lance are plotted in Figure 10 for quantitative analysis. As shown in Figure 10, the effect of increasing CO<sub>2</sub> mixing ratio on pushing away the high temperature zone is more significant than that on reducing the maximum flame temperature. For instance, if the zone with a temperature higher than 3000 K is defined as the high temperature zone, the distance from lance tip to the high temperature zone is 923 mm, 1106 mm, 1471 mm, and 1820 mm respectively, corresponding to the CO<sub>2</sub> mixing ratio of 0, 5 vol.%, 10 vol.%, and 15% vol.%. However, the maximum flame temperature is only reduced from 3150 K to 3063 K when the CO<sub>2</sub> mixing ratio increases from 0 to 15 vol.%.

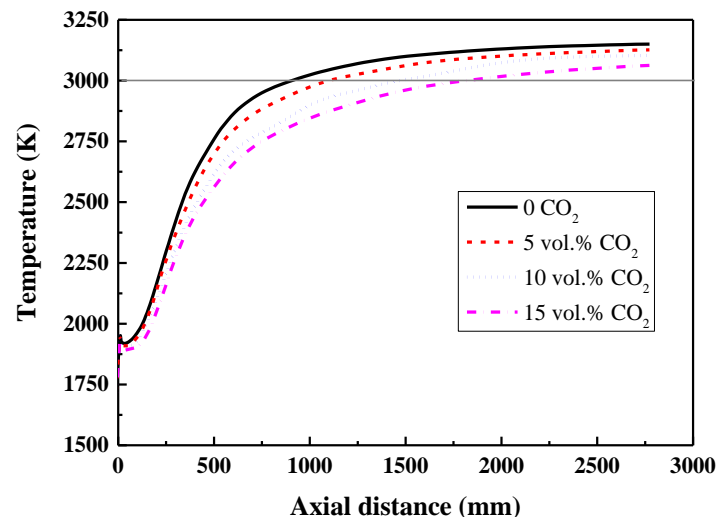


**Figure 10.** Temperature variations on the centerline of the cases with different CO<sub>2</sub>-O<sub>2</sub> mixing ratio.

### 3.2.2. Flow Field Analysis

Velocity field distributions in the longitudinal section of the cases with different CO<sub>2</sub>-O<sub>2</sub> mixing ratio are shown in Figure 11. There is almost no obvious difference that can be seen from Figure 11. Therefore, the velocity distributions on the radial direction 1500 mm away from the lance tip are plotted in Figure 12. It should be noted that the reason for selecting the radial direction 1500 mm from the lance tip is that 1500 mm is the reference lance height used in the steelmaking converter furnace, which is the common distance between lance tip and molten bath surface. Figure 12 also shows that changing CO<sub>2</sub> mixing ratio has little effect on the jet velocity distribution.

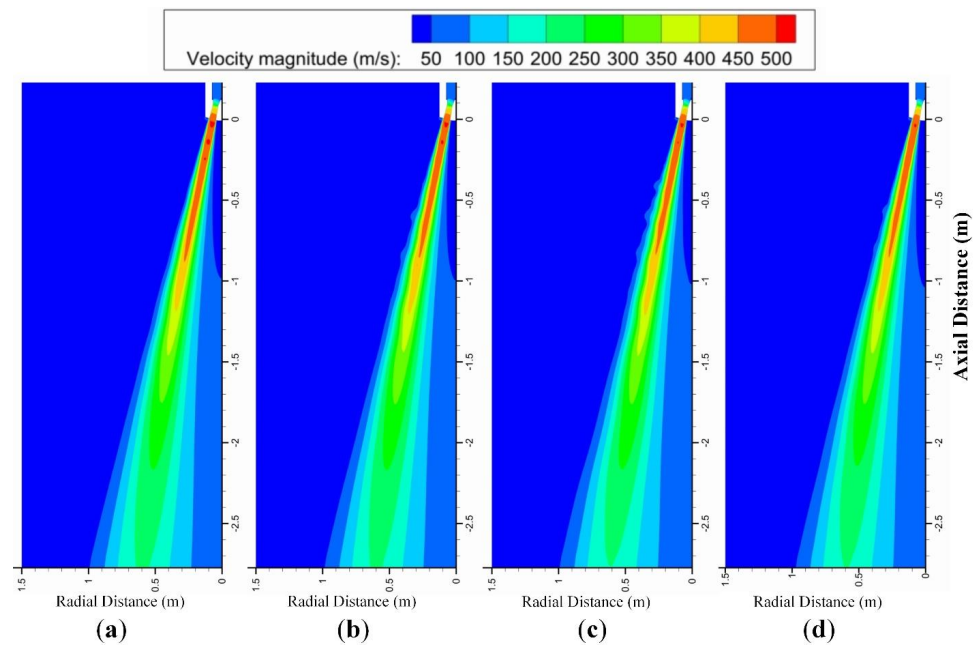


**Figure 11.** Velocity field distributions of the cases with different CO<sub>2</sub>-O<sub>2</sub> mixing ratio: (a) No CO<sub>2</sub> mixed; (b) 5 vol.% CO<sub>2</sub> mixed; (c) 10 vol.% CO<sub>2</sub> mixed; (d) 15 vol.% CO<sub>2</sub> mixed.

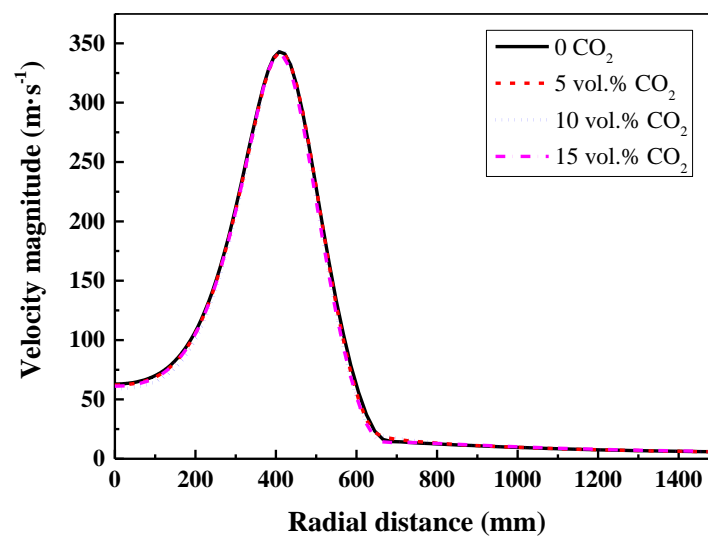


**Figure 12.** Velocity distributions on the radial direction 1500 mm away from the lance tip.

In addition to velocity, dynamic pressure can better evaluate the impact capacity of the jet, which is the product of density and the square of velocity. Dynamic pressure distribution on the radial direction 1500 mm away from the lance tip are plotted in Figure 13.

It can be seen that the influence of CO<sub>2</sub> mixing ratio on dynamic pressure is relatively significant. When the CO<sub>2</sub> mixing ratio increases from 0 to 15 vol.%, maximum dynamic pressure of the jet increased from 23,624 Pa to 25,559 Pa. The main reason for the difference of above laws is that the density of CO<sub>2</sub> is larger than that of O<sub>2</sub>. Molecular weight of the CO<sub>2</sub> is 44, while molecular weight of the O<sub>2</sub> is only 32. Under the condition of similar pressure and temperature, the higher the molecular weight, the higher the density. Based on the definition of dynamic pressure, since the CO<sub>2</sub> mixing ratio has little effect on jet velocity, with the increase of CO<sub>2</sub> mixing ratio, the density of jet increases, and the dynamic pressure of jet increases accordingly.

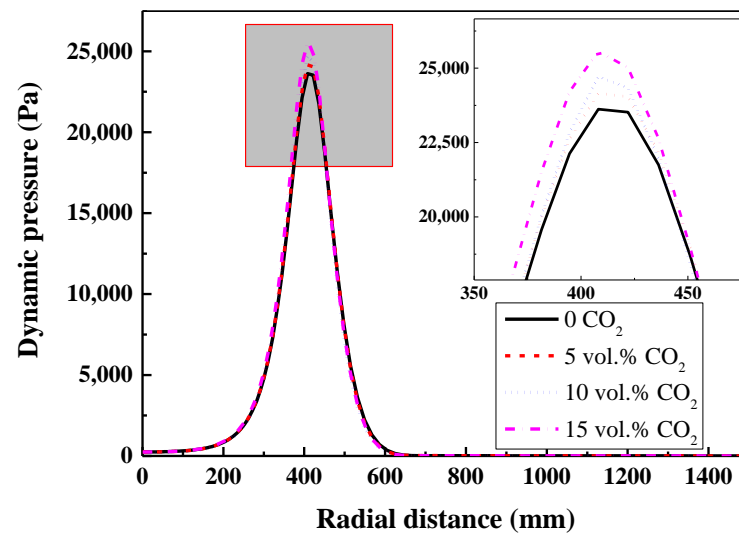


**Figure 13.** Dynamic pressure distributions on the radial direction 1500 mm away from the lance tip.

In conclusion, although increasing the CO<sub>2</sub> mixing ratio has little effect on the jet velocity distribution, but larger dynamic pressure of the jet at the molten bath surface can be obtained, which means stronger impact capacity of the jet.

#### 4. Industrial Experiment

##### 4.1. Experimental Conditions

After knowing well the jet characteristics of converter oxygen lance blowing CO<sub>2</sub>-O<sub>2</sub> mixed gas, an industrial experiment was carried out in a 120-ton converter to check out its practical application performance, especially the dephosphorization effect. Structure and dimensional parameters of the oxygen lance installed in the converter are the same as the geometric model used in the simulation, just as shown in Figure 1. In fact, the picture of oxygen lance shown in Figure 1b was taken in the converter steelmaking plant. A small and temporary CO<sub>2</sub> gas source station was built to supply the CO<sub>2</sub> for top blowing. Limited by the CO<sub>2</sub> supply capacity, it was difficult to blow CO<sub>2</sub> for a long time. At the same time, in order to eliminate the interference of other factors, this experiment was designed to blow CO<sub>2</sub>-O<sub>2</sub> mixed gas only in the dephosphorization period, and blow pure oxygen in the rest time just as usual. Based on the CO<sub>2</sub> supply capacity and the optimal dephosphorization time, the mixing ratio of CO<sub>2</sub> in CO<sub>2</sub>-O<sub>2</sub> mixed gas was designed to be 15 vol.%, and the blowing time was designed to be the period of 120~300 s after the start of oxygen blowing. The reason why CO<sub>2</sub> was not mixed immediately after the start of blowing was that quick temperature rise and quick slagging were required at the initial stage of blowing, but mixing CO<sub>2</sub> will have unfavorable effect.

During the period of 120~300 s after the start of blowing, the total flow rate of CO<sub>2</sub>-O<sub>2</sub> mixed gas was 24,000 Nm<sup>3</sup>·h<sup>-1</sup>. According to the theoretical calculation, about 1.5 Nm<sup>3</sup> CO<sub>2</sub> was consumed for smelting 1-ton molten steel. Apart from mixing CO<sub>2</sub> in the above-mentioned period, other operation modes remain the same as before. During the ex-

periment, the averaged charge amount of hot metal and scrap was 106 ton and 28 ton, respectively. Composition and temperature of the hot metal are shown in Table 2.

**Table 2.** Composition and temperature of the hot metal during industrial experiment.

	[C], wt. %	[Si], wt. %	[Mn], wt. %	[P], wt. %	[S], wt. %	T, K
Fluctuation range	3.79~4.35	0.48~0.81	0.59~0.83	0.098~0.143	0.029~0.057	1537~1596
Average value	4.13	0.67	0.70	0.116	0.043	1578

#### 4.2. Experiment Results

Finally, 67 heats of converter steelmaking were finished in this industrial experiment. In order to eliminate the influence of steel grade, only those heats with tapping [C] content of 0.4~0.5 wt.% are analyzed, totaling 41 heats. As a contrast, 41 heats smelted just before the experiment are presented. End-point [P] content and dephosphorization rate of every heat are shown in Figure 14. First, a simple statistics *t*-test was made for the two groups of experimental data. For the data of end-point [P] content, the calculated *P* value is 0.00062, and the calculated *P* value for the data of dephosphorization rate is 0.0047, indicating that the difference before and after mixing CO<sub>2</sub> is very significant. From Figure 14, it can be seen that better dephosphorization performance is achieved by mixing CO<sub>2</sub> into the oxygen, the averaged end-point [P] content is reduced from 0.0155 wt.% to 0.0129 wt.%, and the averaged dephosphorization rate is increased from 86.8% to 88.3%. By the way, after blowing CO<sub>2</sub>-O<sub>2</sub> mixed gas, the fluctuation range of end-point [P] content becomes smaller, indicating that the dephosphorization also gets more stable. The main reason for better dephosphorization performance should be the better stirring and better thermodynamic conditions provided by mixing CO<sub>2</sub> during the dephosphorization period. On the other hand, due to the endothermic effect of CO<sub>2</sub>, averaged end-point temperature decreases slightly, which is also beneficial to the phosphorus removal. For those heats with tapping [C] content of 0.4~0.5 wt.%, the averaged tapping temperature is reduced from 1922 K to 1914 K.

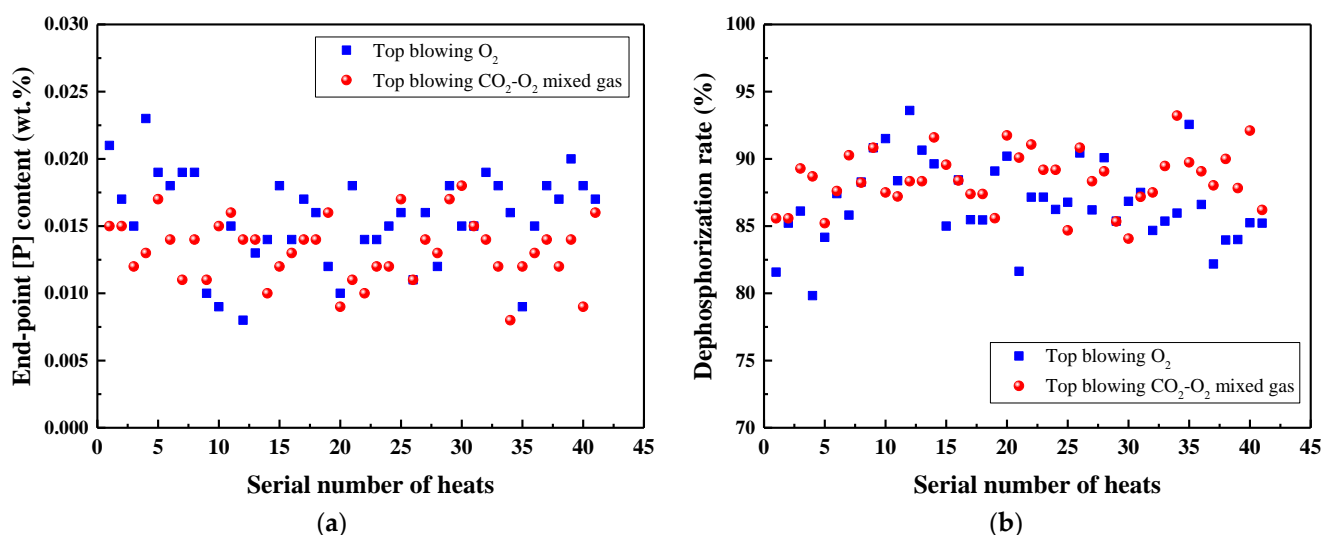


**Figure 14.** Dephosphorization performance during industrial experiment: (a) end-point [P] content; (b) dephosphorization rate.

#### 5. Conclusions

The Eddy Dissipation Concept model coupled with detailed chemical mechanism was used in the present simulation work to study the combustion features between of multiple supersonic jets and ambient high-temperature CO atmosphere, as well as its influence on

the jet characteristics. Then the effects of mixing CO<sub>2</sub> into the oxygen jets were discussed in detail. The conclusions are as follows:

- (1) There is significant difference in the temperature field before and after activating the combustion model. Combustion reaction between the supersonic oxygen jet and the ambient environment occurs, forming the combustion flame. The combustion flame is mainly distributed in the area between multiple jets. For the multi-nozzle oxygen lance, inner side of the supersonic jet is easier to be ignited than the outer side.
- (2) The combustion reaction can hardly affect the high-velocity region of the jet. While the influence of combustion on low-velocity region of the jet is obvious, both the velocity of jet and the diameter of jet increase obviously. Overall, the combustion reaction has a noticeable influence on the jet characteristics, which should not be ignored.
- (3) Maximum temperature of the combustion flame decreases slightly with the increase of CO<sub>2</sub> mixing ratio. More importantly, as the CO<sub>2</sub> mixing ratio increases, the high temperature zone of combustion flame moves away from the lance tip significantly, which is beneficial to reduce the heat flux intensity of lance tip and prolong the service life of oxygen lance.
- (4) Although the increase of CO<sub>2</sub> mixing ratio has little effect on the jet velocity distribution, but larger dynamic pressure of the jet at the molten bath surface can be obtained, which means stronger impact capacity of the jet.
- (5) The industrial experiment shows that better dephosphorization performance can be achieved by mixing 15 vol.% CO<sub>2</sub> into the oxygen during the dephosphorization period, the averaged end-point [P] content is reduced from 0.0155 wt.% to 0.0129 wt.%, and the fluctuation range of end-point [P] content becomes smaller.

**Author Contributions:** Conceptualization, S.H. and R.Z.; methodology, S.H. and J.T.; software, S.H.; validation, G.W., J.T. and Q.Z.; formal analysis, G.W. and C.Z.; investigation, C.Z.; resources, D.W.; data curation, C.Z.; writing—original draft preparation, G.W.; writing—review and editing, S.H.; visualization, J.T.; supervision, D.W. and R.Z.; project administration, S.H.; funding acquisition, S.H. and J.T. All authors have read and agreed to the published version of the manuscript.

**Funding:** This research was funded by the National Natural Science Foundation of China (No. 52104337 and 52074186); Natural Science Foundation of Jiangsu Province (No. BK20200869).

**Data Availability Statement:** Not applicable.

**Conflicts of Interest:** The authors declare no conflict of interest.

## References

1. Li, Q.; Chen, Z.A.; Zhang, J.T.; Liu, L.C.; Li, X.C.; Jia, L. Positioning and revision of CCUS technology development in China. *Int. J. Greenh. Gas Con.* **2016**, *46*, 282–293. [[CrossRef](#)]
2. Wang, Y.; Guo, C.H.; Chen, X.J.; Jia, L.Q.; Guo, X.N.; Chen, R.S.; Zhang, M.S.; Chen, Z.Y.; Wang, H.D. Carbon peak and carbon neutrality in China: Goals, implementation path and prospects. *China Geol.* **2021**, *4*, 720–746. [[CrossRef](#)]
3. Mannion, F.J.; Fruehan, R.J. Decarburization kinetics of liquid Fe–C<sub>sat</sub> alloys by CO<sub>2</sub>. *Metall. Mater. Trans. B* **1989**, *20*, 853–861. [[CrossRef](#)]
4. Sani, D.R.; Belton, G.R. Interfacial reaction kinetics in the decarburization of liquid iron by carbon dioxide. *Metall. Trans. B* **1976**, *7*, 235–244. [[CrossRef](#)]
5. Nomura, H.; Mori, K. Kinetics of decarburization of liquid iron by Ar–CO<sub>2</sub> gas mixture. *Tetsu—Hagane* **1972**, *58*, 1603–1605. [[CrossRef](#)]
6. Niiri, Y.; Ito, K.; Sano, K. Research on the rates of decarburization and oxidation of molten iron alloys with CO<sub>2</sub>–Ar atmosphere. *Tetsu—Hagane* **1969**, *55*, 437–438. [[CrossRef](#)]
7. Sain, D.R.; Belton, G.R. The influence of sulfur on interfacial reaction kinetics in the decarburization of liquid iron by carbon dioxide. *Metall. Trans. B* **1978**, *9*, 403–407. [[CrossRef](#)]
8. Jin, R.J.; Zhu, R.; Feng, L.X.; Yin, Z.J. Experimental study of CO<sub>2</sub>–O<sub>2</sub> mixed blowing in steelmaking. *J. Univ. Sci. Technol. Beijing* **2007**, *29*, 77–86.
9. Yin, Z.J.; Zhu, R.; Yi, C.; Chen, B.Y.; Wang, C.Y.; Ke, J.X. Fundamental research on controlling BOF dust by COMI steelmaking process. *Iron Steel* **2009**, *44*, 92–95.
10. Yi, C.; Zhu, R.; Chen, B.Y.; Wang, C.R.; Ke, J.X. Experimental research on reducing the dust of BOF in CO<sub>2</sub> and O<sub>2</sub> mixed blowing steelmaking process. *ISIJ Int.* **2009**, *49*, 1694–1699. [[CrossRef](#)]

11. Zhu, R.; Bi, X.R.; Lv, M.; Liu, R.Z.; Bao, X. Research on steelmaking dust based on difference of Mn, Fe and Mo vapor pressure. *Adv. Mater. Res.* **2011**, *284*, 1216–1222.
12. Yi, C.; Zhu, R.; Yin, Z.; Hou, N.; Chen, B.; Wang, C.R.; Ke, J.X. Experimental research of COMI steelmaking process based on 30t converter. *Chin. J. Process Eng.* **2009**, *9*, 228–231.
13. Zhang, W.; Li, Z.Z.; Zhu, R.; Liu, R.Z. Experiment study of CO<sub>2</sub> blowing in steelmaking process. *Ind. Heat.* **2015**, *44*, 41–44.
14. Lv, M.; Zhu, R.; Wei, X.Y.; Wang, H.; Bi, X.R. Research on top and bottom mixed blowing CO<sub>2</sub> in converter steelmaking process. *Steel Res. Int.* **2012**, *83*, 11–15. [[CrossRef](#)]
15. Lv, M.; Zhu, R.; Bi, X.R.; Wei, N.; Wang, C.R.; Ke, J.X. Fundamental research on dephosphorization of BOF by COMI steelmaking process. *Iron Steel* **2011**, *46*, 31–35.
16. Zhu, R.; Han, B.C.; Dong, K.; Wei, G.S. A review of carbon dioxide disposal technology in the converter steelmaking process. *Int. J. Miner. Metall. Mater.* **2020**, *27*, 1421–1429. [[CrossRef](#)]
17. Tago, Y.; Higuchi, Y. Fluid Flow Analysis of Jets from Nozzles in Top Blown Process. *ISIJ Int.* **2003**, *43*, 209–215. [[CrossRef](#)]
18. Lv, M.; Zhu, R.; Guo, Y.G.; Wang, Y.W. Simulation of Flow Fluid in the BOF Steelmaking Process. *Metall. Mater. Trans. B* **2013**, *44*, 1560–1571. [[CrossRef](#)]
19. Higuchi, Y.; Tago, Y. Effect of Lance Design on Jet Behavior and Spitting Rate in Top Blown Process. *ISIJ Int.* **2001**, *41*, 1454–1459. [[CrossRef](#)]
20. Lv, M.; Li, H.; Lin, T.C.; Xie, K.; Xue, K. Behavior of Gas–Slag–Metal Emulsion with Nozzle-Twisted Lance in Converter Steelmaking Process. *Steel Res. Int.* **2021**, *92*, 2100103. [[CrossRef](#)]
21. Lv, M.; Li, H.; Xing, X.D.; Lin, T.C.; Hu, S.Y.; Xie, K. Variation in Multiphase Flow Characteristics by Nozzle-Twisted Lance Blowing in Converter Steelmaking Process. *Steel Res. Int.* **2021**, *93*, 2100409. [[CrossRef](#)]
22. Feng, C.; Zhu, R.; Dong, K.; Wei, G.S.; Han, B.C.; Li, W.F.; Wu, W.H. Effects of Nozzle Layout and Parameters on the Jet Characteristics of a CO<sub>2</sub> + O<sub>2</sub> Mixed Oxygen Lance. *Metall. Mater. Trans. B* **2021**, *52*, 425–439. [[CrossRef](#)]
23. Nonomura, T.; Fujii, K. Overexpansion Effects on Characteristics of Mach Waves from a Supersonic Cold Jet. *AIAA J.* **2011**, *49*, 2282–2294. [[CrossRef](#)]
24. Li, Q.; Li, M.M.; Li, L.; Zou, Z.S. Numerical analysis of oxygen jet characteristic for BOF convertor top-blown process based on CFD method. *J. Northeast Univ. (Nat. Sci.)* **2013**, *34*, 828–831.
25. Li, M.M.; Li, Q.; Kuang, S.B.; Zou, Z.S. Coalescence Characteristics of Supersonic Jets from Multi-Nozzle Oxygen Lance in Steelmaking BOF. *Steel Res. Int.* **2015**, *86*, 1517–1529. [[CrossRef](#)]
26. Alam, M.; Naser, J.; Brooks, G. Computational Fluid Dynamics Simulation of Supersonic Oxygen Jet Behavior at Steelmaking Temperature. *Metall. Mater. Trans. B* **2010**, *41*, 636–645. [[CrossRef](#)]
27. Hu, S.Y.; Zhu, R.; Dong, K. Numerical simulation research on flow fields in combined blown converter at steelmaking temperature. *Chin. J. Eng.* **2018**, *40*, 108–115.
28. Liu, F.H.; Zhu, R.; Dong, K.; Hu, S.Y. Effect of Ambient and Oxygen Temperature on Flow Field Characteristics of Coherent Jet. *Metall. Mater. Trans. B* **2015**, *47*, 228–243. [[CrossRef](#)]
29. Sumi, I.; Okuyama, G.; Nabeshima, S.; Matsuno, H.; Kishimoto, Y. Behavior of Top-Blown Jet under Reduced Pressure. *ISIJ Int.* **2007**, *47*, 73–79. [[CrossRef](#)]
30. Zhao, F.; Zhang, Y.L.; Zhu, R.; Zhu, L.F.; Tian, D.D. Numerical simulation on effect of environment pressure on supersonic oxygen jet characteristics. *China Metall.* **2014**, *24*, 22–25.
31. Gou, H.; Irons, G.A.; Lu, W.K. Mathematical modeling of post combustion in a KOBM converter. *Metall. Trans. B* **1993**, *24*, 179–188. [[CrossRef](#)]
32. Zhao, F.; Liu, F.H.; Sun, D.B. Behaviors of Supersonic Oxygen Multi-jets with various preheating temperatures. *Metall. Mater. Trans. B* **2021**, *52*, 2626–2641. [[CrossRef](#)]
33. Launder, B.E.; Spalding, D.B. *Lectures in Mathematical Model of Turbulence*; Academic Press: London, UK, 1972; p. 124.
34. Hu, S.Y.; Zhu, R.; Dong, K.; Liu, R.Z. Numerical Simulation and Industrial Experimental Research on the Coherent Jet with “CH<sub>4</sub> + N<sub>2</sub>” Mixed Fuel Gas. *Metall. Mater. Trans. B* **2018**, *49*, 2584–2598. [[CrossRef](#)]
35. Li, P.F.; Dally, B.B.; Mi, J.C.; Wang, F.F. MILD oxy-combustion of gaseous fuels in a laboratory-scale furnace. *Combust. Flame* **2013**, *160*, 933–946. [[CrossRef](#)]
36. Li, P.F.; Mi, J.C.; Dally, B.B. Premixed moderate or intense low-oxygen dilution (MILD) combustion from a single jet burner in a laboratory-scale furnace. *Energy Fuels* **2011**, *25*, 2782–2793. [[CrossRef](#)]
37. Mi, J.C.; Li, P.F.; Dally, B.B.; Craig, R.A. Importance of initial momentum rate and air-fuel premixing on moderate or intense low oxygen dilution (MILD) combustion in a recuperative furnace. *Energy Fuels* **2009**, *23*, 5349–5356. [[CrossRef](#)]
38. Mardani, A.; Tabejamaat, S.; Ghamari, M. Numerical study of influence of molecular diffusion in the MILD combustion regime. *Combust. Theor. Model* **2010**, *14*, 747–774. [[CrossRef](#)]
39. Christo, F.C.; Dally, B.B. Modeling turbulent reacting jets Issuing into a hot and diluted coflow. *Combust. Flame* **2005**, *142*, 117–129. [[CrossRef](#)]
40. Hu, S.Y.; Zhu, R.; Dong, K.; Wu, W.H. New Process for Resource Utilization of Converter Gas and Simulation on the Combustion of Converter Gas. *ISIJ Int.* **2018**, *58*, 776–783. [[CrossRef](#)]
41. Chui, E.H.; Raith, G.D. Computation of radiant heat transfer on a nonorthogonal mesh using the finite-volume method. *Numer. Heat Transf. B-Fundam.* **1993**, *23*, 269–288. [[CrossRef](#)]